6 FATIGUE LIFE EVALUATION OF PLANT YARN REINFORCED COMPOSITES*

6.1 Introduction

Fatigue loads are often 'normal operation' loads for many structural applications, including wind turbine blades, buildings, bridges, helicopters and aeroplanes (Fig. 6.1) [1]. In general, fatigue occurs when a material is subjected to repeated, variable/constant amplitude loading-unloading-reloading cycles, over a period of time. The fatigue life of a material, defined as the number of cycles to failure, is dependent on several factors including stress level, stress state, mode of cycling, process history, material composition, dimension and geometry, load history, environmental conditions, and lastly, by the mutual influence of all these parameters [2]. Importantly, the fatigue strength of a material (or the nominal maximum stress S_{max} a material can endure under cyclic loads) is less than the ultimate stress limit S_0 (under static loads). Moreover, S_{max}/S_0 reduces with increasing number of load cycles. Hence, if a material is to be employed in a fatigue critical component, it is imperative that its response to cyclic loads is well-characterised.

Natural fibres for composite applications have become a topic of growing interest. Although the usage of plant fibre composites (PFRPs) is on the rise, certain aspects of their behaviour are still inadequately understood or investigated. To date, there exists neither an adequate database of PFRPs subjected to cyclic loads (in the form of stress-life diagrams and lifetime data), nor an adequate fatigue lifetime prediction methodology (in the form of constant-life diagrams) for structures built from PFRPs. On the other hand, the fatigue behaviour of E-glass composites (GFRPs) is well-

Shah DU, Schubel PJ, Licence P, Clifford MJ, Fatigue life evaluation of aligned plant fibre composites through S-N curves and constant-life diagrams. *Composites Science and Technology*, 2013, 74: p. 139-149.

DU Shah Page | 169

^{*} This chapter is based on the peer-reviewed journal article:

documented. This seriously limits the prospective use of PFRPs, and the potential replacement of GFRPs, in fatigue critical structural components.

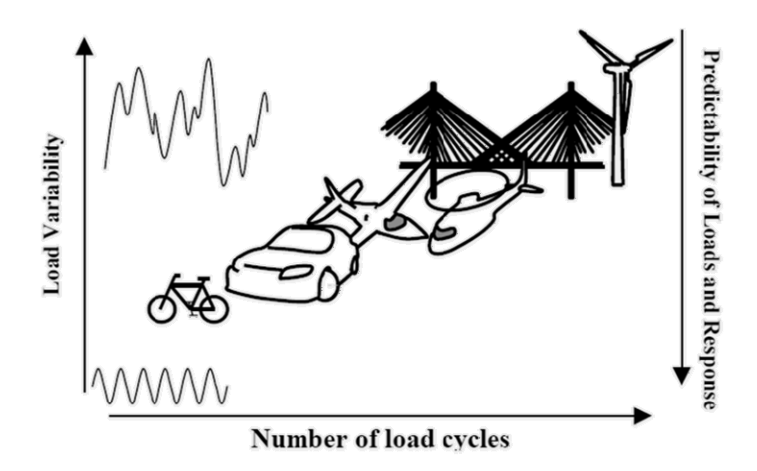


Fig. 6.1. The severity of fatigue in structural components depends on *i*) load variability, *ii*) number of load cycles, and *iii*) predictability of loads and component response [1].

6.2 LITERATURE REVIEW

A few researchers have attempted to uncover the fatigue behaviour of plant fibres and their composites. Investigating the cyclic loading behaviour of single plant leaf fibres, Spatz *et al.* [3] observed that the fibre elastic modulus increased with subsequent loading cycles due to the progressive reorientation of the cellulose microfibrils towards the loading direction. Baley [4] and Silva *et al.* [5] also reported this strain hardening behaviour for flax and sisal fibres, the majority of which occurs during the early stages of cyclic deformation. For instance, the flax fibre elastic modulus can increase by 60-80% between the 1st and the 200th cycle (from 40 GPa to 72 GPa) [4]. With an average ultimate tensile strength (UTS) of 400 MPa, sisal fibres can survive at least 10^6 cycles when subjected to a ratio of maximum applied fatigue stress to ultimate tensile strength S_{max}/UTS of 0.5 [5]. The slope of the S-N curve for a single sisal fibre is approximately 9% of the UTS per decade of cycles [5]. In comparison, E-glass fibres with average UTS of 2130 MPa survive at least 10^6 cycles when subjected to a higher ratio S_{max}/UTS of 0.8 with their fatigue strength degrading at a slower rate of 3% per decade of cycles [6].

The fatigue fracture surface of plant fibres shows formation of micro-cracks in the secondary cell wall (perpendicular to the load), followed by subsequent propagation to the middle lamellae and delamination between adjacent fibres [5, 7]. In addition, a characteristic peeling-off of the primary/secondary cell wall layers is also observed, due to degradation of the cellulosic fibrillar structure and the weakening of the cellulose/lignin-hemicellulose interface, with increasing number of load cycles [5, 7].

The fatigue deformation mechanism of a fibre reinforced composite is more complex and largely dependent on strain development and damage accumulation at the fibre/matrix interface [8]. Unlike metals, composite materials are inhomogeneous and anisotropic. While fatigue in metals is a localised process involving the nucleation and growth of a dominant crack to unstable failure, fatigue in composites occurs in a general fashion due to the gradual accumulation and interaction of dispersed damage [8].

Recently, Liang *et al.* [9] compared the tension-tension (stress ratio of R = 0.1) fatigue behaviour of biaxial flax/epoxy and glass/epoxy composites. The authors found that while glass/epoxy composites exhibit a higher resistance to fatigue loading due to their higher static strength, the stress-life (S-N) curve of glass/epoxy is much steeper implying a more significant decrease in fatigue strength with respect to cycles to failure. In fact, the fatigue stress level drops by 57 and 21 MPa every decade of cycles for [0,90] and $[\pm 45]$ glass/epoxy composites, but by only 25 and 7 MPa every decade for [0,90] and $[\pm 45]$ flax/epoxy composites. In composite materials, fatigue damage does not always immediately reduce the strength of the composite, although it often reduces the stiffness [8]. Liang *et al.* [9] reported that while the stiffness of glass/epoxy composites reduced by 7-25% and 50-70% for [0,90] and $[\pm 45]$ samples, flax/epoxy composites offered a more stable fatigue performance during their fatigue life with a stiffness increase of 2% or decrease of only 15-20% for [0,90] and $[\pm 45]$ samples, respectively.

In an extensive study on fibre and interface parameters affecting the tension-tension fatigue behaviour of PFRPs, Gassan [10, 11] recorded the dynamic stress-strain curve and calculated the specific damping capacity SDC (ratio of energy dissipated

every cycle to the initial maximum strain energy [11]) as a value indicative of progressive material damage. However, a material SDC-load curve is not useful when designing against fatigue. Nonetheless, the author found that PFRPs manufactured with *i*) fibres of higher strength and modulus, *ii*) improved fibre/matrix interface through fibre surface treatment, *iii*) unidirectional plies rather than woven biaxial architecture, or *iv*) higher fibre volume fractions, possess *a*) higher damage initiation loads, *b*) comparable or lower damage propagation rates, and *c*) higher failure loads.

Towo and Ansell [12, 13] conducted a more classic study on the fatigue properties of unidirectional sisal fibre thermoset matrix composites, presenting data in the more convenient format of S-N diagrams and constant life diagrams, albeit for only two stress ratios. Studying the effect of fibre alkali treatment, they observed that treated fibre composites exhibit better load carrying capacities in tension-tension (R = 0.1) and tension-compression (R = -1) fatigue, for up to $\sim 10^8$ cycles. This is due to improved adhesion between the fibre and the matrix upon fibre treatment, which is confirmed by the smaller damping capacity (area of the stress-strain hysteresis loop) for treated fibre composites. However, Towo and Ansell [12, 13] do declare that treated fibre composites exhibit a steeper slope in their S-N curve compared to untreated fibre composites.

Finally, Isaac and co-workers [14-16] have looked into the fatigue properties of non-woven random mat hemp/polyester composites subjected to *i*) fibre alkali treatment, *ii*) low-velocity impact damage, and *iii*) water immersion. They observed that while composites made from 1% and 5% NaOH treated hemp fibres showed an improvement in the fatigue performance compared to untreated hemp fibre composites, the fatigue properties of composites made from 10% NaOH treated hemp fibres was comparable to that of untreated hemp fibre composites. In addition, while it was expected that the fatigue performance of impact damaged hemp composites would be extremely poor, it was surprising to discover that water immersion had negligible effect on the S-N curve of the hemp/polyester composite.

At present, there are limited papers that enable the preliminary design of PFRPs against fatigue. The objective of this study is to provide a complete set of fatigue data on aligned PFRPs to enable the design of a PFRP component against fatigue. A primary aim of the study described in this chapter is to thoroughly characterise the fatigue performance of aligned PFRPs through S-N lifetime diagrams, and specifically investigate the effect of *i*) plant fibre type, *ii*) fibre volume fraction, *iii*) textile architecture, and *iv*) stress ratio, on PFRP cyclic loading behaviour. At each stage, the fatigue performance of PFRPs is compared to that of E-glass/polyester composites (material data from [17]). In addition, to facilitate fatigue life prediction of a PFRP component, a comprehensive constant-life diagram is generated. Recently, the author of this thesis has applied the data for the fatigue design and life prediction of a 3.5-meter hemp/polyester rotor blade [18, 19].

6.3 EXPERIMENTAL METHODOLOGY

6.3.1 Reinforcement materials

Four commercially available plant fibre yarns/rovings were used as composite reinforcements. The yarns employed in this study are the same as those used in the study described in *Chapter 3*. The material properties of the four yarns are tabulated in Table 6.1. The yarns are denoted according to their fibre type and twist level; so, J190 is a jute yarn with a twist level of 190 tpm. The selected yarns enabled studying the effect of fibre type (jute, hemp and flax) and fibre quality (F50 and F20) on PFRP fatigue performance. Note that fibre quality is defined 'qualitatively' by the source of the fibre/yarn and the mechanical properties of the resulting composite. F50 and F20 yarns/rovings are obtained from different sources (Table 6.1) and the static strength of composites made from the yarns are very different (Table 6.2). Here, F20 is considered as a yarn with high-quality fibres, while F50 is a yarn with low-quality fibres.

For use as aligned reinforcements, the yarns were processed in the form of unidirectional mat and stitched biaxial fabric. Unidirectional (0°) mats were prepared from all the four yarns using a simplified drum winding facility and hydroxyethylcellulose binding agent (Cellosize HEC QP-52000H supplied by Dow

Chapter 6

Chemical), as described in *Chapter 3*. Formax (UK) Ltd also produced 300 gsm stitched biaxial (±45°) fabric from the F50 yarn. This enabled studying the effect of textile architecture on the fatigue behaviour of F50 flax fibre composites.

Table 6.1. List of plant fibre material and their properties (means \pm stdev).

| Yarn ID | Fibre Type | Supplier | Density [†] [gcm ⁻³] | Linear density [†] [tex] | Twist level [†] [tpm] |
|------------|---------------|--|--|---|--------------------------------------|
| J190 | Jute | Janata and Sadat Jute Ltd (Bangladesh) | 1.433 ± 0.005 | 206 ± 21 | 190 |
| H180 | Hemp | Safilin (Poland) | 1.531 ± 0.003 | 278 ± 17 | 180 |
| F50 | Flax | Composites Evolution (UK) | 1.529 ± 0.003 | 229 ± 22 | 50 |
| F20 | Flax | Safilin (France) | 1.574 ± 0.004 | 396 ± 16 | 20 |

[†]Measured in *Chapter 3 and Appendix A*.

6.3.2 Composite manufacture

Aligned composite laminates (250 mm square, 3-3.5 mm thick) were fabricated using the vacuum infusion technique in an aluminium mould tool. The reinforcement mats/fabrics were used as-received (without any preconditioning). Resin infusion was carried out at 70-80% vacuum (200-300 mbar absolute) under ambient temperature. The manufacturing process has been described in detail in *Chapter 3*. All composites were made with unsaturated polyester (Reichhold Norpol type 420-100) as the matrix. The resin was mixed with 0.25 wt% NL49P accelerator (1% Cobalt solution) and 1 wt% Butanox M50 MEKP initiator. Post cure was carried out at 55 °C for 6 h after ambient cure for 16 h. From the manufacturer's datasheet, the resin has a cured density ρ_m of 1.202 gcm⁻³.

As tabulated in Table 6.2, composites with different i) yarn/fibre types (J190, H180, F50 and F20 in $[0]_4$ layup), ii) fibre volume fractions ($[0]_{2-5}$ layup of J190 generating four different fibre volume fractions in the range of 17-38%), and iii) textile architectures (F50 in $[0]_4$, $[\pm 45]_4$, and $[90]_4$ layups), were fabricated by the abovementioned procedure.

The fibre weight fraction w_f of a laminate was calculated using the ratio of the mass of the preform and the resulting composite laminate. The composite density ρ_c was measured using helium pycnometry (minimum of 5 samples). The composite fibre volume fraction v_f was then determined using Eq. 6.1, allowing for porosity v_p . Note the consistency in fibre/matrix volume fractions and the low void content (with the exception of J190 [0]₄) of the PFRPs produced (Table 6.2).

$$v_f = \frac{\rho_c}{\rho_f} w_f; \quad v_m = \frac{\rho_c}{\rho_m} (1 - w_f); \quad v_p = 1 - (v_f + v_m)$$
 Eq. 6.1

For all studies in this thesis, all composite samples were stored for at least 48 hours at ambient conditions before any testing. In addition, all testing was conducted under ambient conditions (typically, 10-20 °C and 60-90% relative humidity).

6.3.3 Mechanical testing

6.3.3.1 Static tests

In order to determine the stress levels for fatigue testing, the static ultimate strengths of the different composites needed to be measured. The ultimate tensile strength UTS was measured for all the composites through static tensile tests, conducted according to ISO 527-4:1997, on an Instron 5985 testing machine equipped with a 100 kN load cell. Six specimens were tested for each type of composite at a cross-head speed of 2 mm/min. While all specimens were 250 mm long, specimens from unidirectional and biaxial composites had a different width of 15 mm and 25 mm, respectively. The physical and tensile properties of the composites are presented in Table 6.2.

The ultimate compressive strength UCS of H180/polyester was measured through static compression tests, conducted according to ASTM D3410, on an Instron 5581 testing machine equipped with a 50 kN load cell and a compression test fixture. Six specimens (140 mm long, 15 mm wide) were tested at a cross-head speed of 1 mm/min. The test fixture and selected gauge length of 12.7 mm prevent the specimen from buckling. The test specimens were speckle-coated prior to testing, enabling longitudinal/transverse strain measurement using a camera. The UCS of H180/polyester composite was measured to be 95.1 ± 6.9 MPa.

Table 6.2. Physical and mechanical (static and fatigue) properties (means \pm stdev) of the fabricated composite laminates.

| Test | Fibre | | Fibre volume fraction | Composite density | Void volume fraction | Experimental ultimate Strength UTS/(UCS) | Fatigue stress ratio R tested | Theoretical single cycle ultimate strength | Fatigue strength coefficient |
|-----------------------------|-------|--------------|-----------------------------|------------------------|----------------------------|---|--|--|------------------------------------|
| Variable | type | Layup | v_f [%] | ρ [gcm ⁻³] | v_p [%] | [MPa] | under | $S_{\theta} [MPa]^{\Psi}$ | <i>b</i> ^Ψ |
| | J190 | $[0]_4$ | 31.7 ± 0.1 | 1.225 ± 0.002 | 4.2 ± 0.8 | 175.1 ± 10.3 | 0.1* | 211.3 | -0.0657 |
| Fibre type | H180 | $[0]_4$ | 35.6 ± 0.8 | 1.303 ± 0.006 | 1.3 ± 0.4 | 171.3 ± 6.5 | 0.1* | 196.4 | -0.0623 |
| | F50 | $[0]_{4}$ | 27.7 ± 0.3 | 1.282 ± 0.004 | 0.9 ± 0.3 | 143.0 ± 6.8 | 0.1* | 164.3 | -0.0739 |
| | F20 | $[0]_{4}$ | 26.9 ± 0.1 | 1.291 ± 0.006 | 0.9 ± 0.4 | 236.3 ± 12 | 0.1* | 297.4 | -0.0690 |
| Fibre volume fraction | J190 | $[0]_{2}$ | 17.1 ± 0.1 | 1.238 ± 0.003 | 0.3 ± 0.2 | 90.2 ± 9.9 | 0.1* | 99.8 | -0.0585 |
| | J190 | $[0]_{3}$ | 25.2 ± 0.1 | 1.251 ± 0.004 | 0.7 ± 0.3 | 140.7 ± 7.7 | 0.1^{*} | 173.5 | -0.0656 |
| | J190 | $[0]_{4}$ | 31.7 ± 0.1 | 1.225 ± 0.002 | 4.2 ± 0.8 | 175.1 ± 10.3 | 0.1^{*} | 211.3 | -0.0657 |
| | J190 | $[0]_{5}$ | 37.8 ± 0.1 | 1.276 ± 0.002 | 1.1 ± 0.2 | 224.7 ± 26.5 | 0.1* | 262.6 | -0.0669 |
| | F50 | $[0]_{4}$ | 27.7 ± 0.3 | 1.282 ± 0.004 | 0.9 ± 0.3 | 143 ± 6.8 | 0.1* | 164.3 | -0.0739 |
| Textile architecture | F50 | $[\pm 45]_4$ | 28.9 ± 0.1 | 1.293 ± 0.005 | 0.3 ± 0.2 | 51.4 ± 2.8 | 0.1* | 73.7 | -0.0872 |
| | F50 | $[90]_4$ | 25.8 ± 0.3 | 1.278 ± 0.004 | 0.7 ± 0.2 | 13.2 ± 0.4 | 0.1* | 19.8 | -0.0698 |
| | H180 | $[0]_4$ | 35.6 ± 0.8 | 1.303 ± 0.006 | 1.3 ± 0.4 | 171.3 ± 6.5 | 0.1* | 196.4 | -0.0623 |
| | H180 | $[0]_{4}$ | 35.6 ± 0.8 | 1.303 ± 0.006 | 1.3 ± 0.4 | 171.3 ± 6.5 | 0.3^{*} | 234.8 | -0.0548 |
| Stress ratio | H180 | $[0]_{4}$ | 35.6 ± 0.8 | 1.303 ± 0.006 | 1.3 ± 0.4 | 171.3 ± 6.5 | 0.5^{*} | 255.4 | -0.0526 |
| | H180 | $[0]_{4}$ | 35.6 ± 0.8 | 1.303 ± 0.006 | 1.3 ± 0.4 | (95.1 ± 6.9) | -1 [†] | (161.7/50.5) | -0.1567/-0.03 |
| | H180 | $[0]_{4}$ | 35.6 ± 0.8 | 1.303 ± 0.006 | 1.3 ± 0.4 | (95.1 ± 6.9) | 2.5^{\ddagger} | (124.4) | -0.0373 |

^{*}Tension-Tension (TT) mode; †Tension-Compression (TC) mode; ‡Compression-Compression (CC) mode

 $^{^{\}Psi}$ S_0 and b are material fatigue parameters described in Section 6.3.3.2.3 and Eq. 6.2. They are obtained by fitting Eq. 6.2 on the fatigue data obtained for each material tested under the different fatigue stress ratios R.

6.3.3.2 Fatigue tests

Specimen preparation

Rectangular test specimens were obtained by cutting the composite laminates with a high-speed abrasive/diamond cutting machine. To avoid moisture intake, lubrication fluid was not used during cutting of the PFRP specimens. Upon cutting, all edges and ends were polished and roughened, respectively, with 600 grit sand paper. Aluminium end-tabs (50 mm long, 1 mm thick) were then glued to the specimens using Araldite Rapid adhesive, to protect the specimen surface from damage from the jaws of the test machine.

Table 6.2 states which composites were tested in tension-tension (TT) mode, tension-compression (TC) mode and compression-compression (CC) mode. For tests in TT mode, test specimens were 250 mm long and 15 mm wide with a gauge length of 150 mm. For tests in TC and CC modes, test specimens were 120 mm long and 15 mm wide with a gauge length of 11.5 mm. The smaller gauge length of specimens tested in TC/CC modes ensured that the specimens didn't buckle under compressive loads.

Test parameters

Fatigue tests were performed on an Instron 8801 servo-hydraulic testing machine under load-control mode. The calibrated load cell had a force rating of ± 100 kN and accuracy of 0.047 kN. Constant amplitude loads were applied in a sinusoidal waveform at a frequency of 10 Hz. BS ISO 13003:2003 [20] advices that while high testing frequencies (of up to 25 Hz) are desirable, to avoid self-generated heating in the specimen, for rate-dependent materials the rise in specimen surface temperature should normally be limited to 10 °C during the test. BS ISO 13003:2003 [20] does highlight that the limit of 10 °C does not apply to rapid temperature rises associated with final failure. Gassan *et al.* [10, 11, 21] observed that for woven and unidirectional flax/jute composites with a fibre content of 22-40% (similar to this study), a test frequency of 10 Hz led to a temperature rise of less than 7 °C. As is common practise in fatigue testing [12, 22, 23], all tests in this study were conducted in ambient laboratory air (typically, 15-20 °C and 60-90% relative humidity).

DU Shah Page | 177

Chapter 6

Preliminary tests were conducted to determine an optimised jaw pressure (of 20 bar) to grip the specimens. This enabled minimising the number of specimens that failed at the jaw. TT mode (R = 0.1) fatigue tests were carried out on all composite samples (Table 6.2). To study the effect of stress ratio R on fatigue performance and to then generate a complete constant-life diagram for H180 composites, only they were studied under five different stress ratios: R = 0.1, 0.3, 0.5 in TT mode, R = -1 in TC mode, and R = 2.5 in CC mode (Table 6.2). Fig. 6.2 presents example load waveforms used for fatigue testing, showing definition of terms and illustration of R-values. Anti-buckling guides were not used during TC/CC loading as they could cause extra heating of the specimen [24].

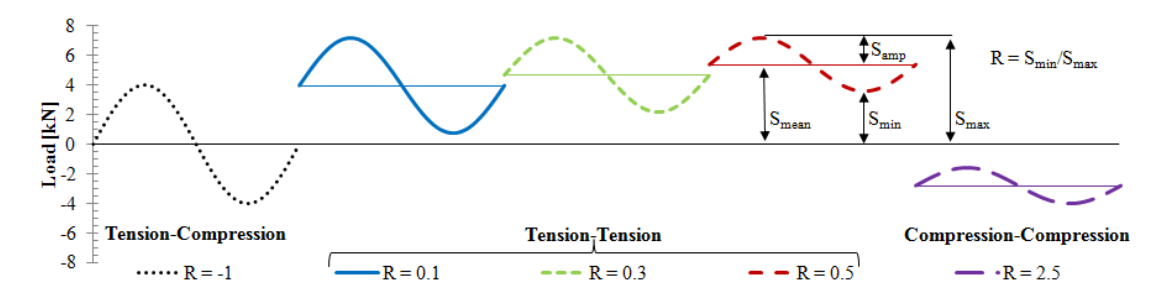


Fig. 6.2. Example sinusoidal constant amplitude load waveforms showing definition of terms and illustration of R-values (for a constant S_{max} of 90% of the UTS or UCS).

In accordance with BS ISO 13003:2003 [20], at least five specimens were tested to failure at a minimum of five levels of maximum (absolute) stress S_{max} (eg. 90%, 80%, 70%, 60%, 50% and 45% of UTS or UCS), up to at least 10^6 cycles, for the determination of the material S-N lifetime diagram. Specimens with failures initiated in the tab area were not included in the data. While the number of specimens tested do not allow a statistical analysis, they are sufficient for such exploratory investigations [20].

Data analysis

As illustrated in Fig. 6.3, after plotting Wohler stress-life (S-N) diagrams, power-law regression equations (Eq. 6.2) were determined for each material, where S_{max} is the maximum (absolute) stress applied, N is the number of cycles to failure, S_0 is the

single cycle (static) ultimate strength of the material, and b is the material fatigue strength coefficient. Eq. 6.2 yields a linear S-N curve on a log-log plot.

Table 6.2 presents material fatigue parameters (S_0 and b) based on Eq. 6.2, for each material tested under the different fatigue stress ratios R. The material fatigue strength coefficient b is a very useful parameter; a smaller value of b implies a steeper slope of the logS-logN curve and thus faster fatigue strength degradation every decade of cycles. For reference, Eq. 6.2 derives from the integration of the Paris fatigue crack growth rate law (Eq. 6.3) through the substitution of Eq. 6.4, where a is the crack length, K is the (maximum) stress intensity factor, and A and Y are constants. Note that b is the same in Eq. 6.2 and Eq. 6.3.

The trend in S-N lifetime data can also be described by Eq. 6.5, where c (like b) is a material constant. Generally, S-N data for composites may follow either Eq. 6.2 or Eq. 6.5 or both, depending on the material system [22]. As the power-law regression curve of Eq. 6.2 is found to be a better fit to the experimental results, it is used here.

$$S_{\text{max}} = S_0 N^b$$
 Eq. 6.2

$$\frac{da}{dN} = AK^{-(1/b)}$$
 Eq. 6.3

$$K = SY\sqrt{\pi a}$$
 Eq. 6.4

$$S_{\text{max}} = S_0 (1 - c \log N)$$
 Eq. 6.5

While static strength was plotted on the S-N diagram at N=1 (Fig. 6.3), it was ignored when obtaining the power-law regressions representing the trend in S-N data for three prime reasons. Firstly, the static data was obtained at a strain rate an order of magnitude below the fatigue strain rate. Secondly, the failure mechanism of a static failure is fundamentally different to a fatigue failure [1]. Thirdly, as including the static strength data weakened the strength of the regression (indicated by the R^2 -value), its omission is reasonable, particularly as low-cycle fatigue ($N < 10^3$) is usually of little interest.

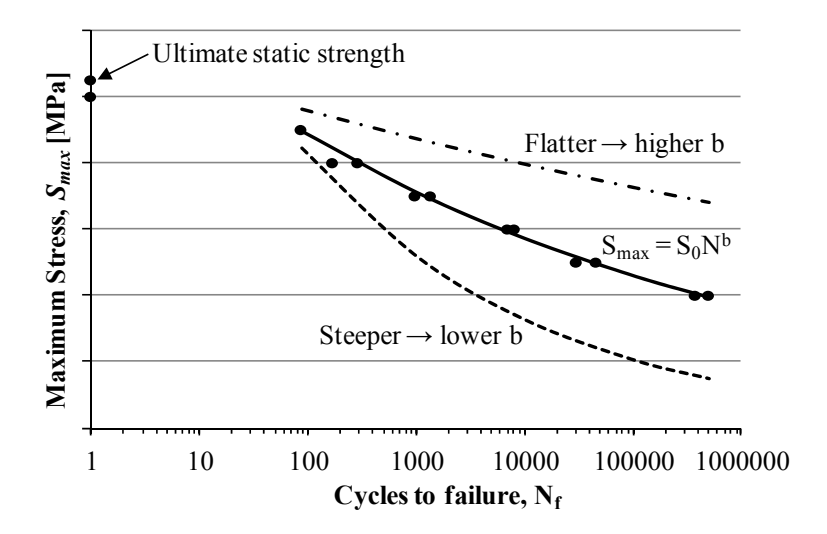


Fig. 6.3. Typical S-N lifetime diagram with example data following a power-law regression curve, where b is the material fatigue strength coefficient.

A complete Haigh constant-life diagram was then constructed using data obtained from the power-law regression lines, of the S-N diagrams, for H180/polyester composite specimens tested under the five different stress ratios. A constant-life diagram plots the mean stress S_{mean} along the x-axis and stress amplitude S_{amp} along the y-axis. The combination of amplitude stress S_{amp} and mean stress S_{mean} were determined for each decade of fatigue cycles (eg. 10^2 , 10^3 , 10^4 and so on), for the five stress ratios. Lines of constant life were drawn through the corresponding data points; no curve fitting was used. The static failure conditions, *i.e.* the end points on the x-axis, were defined by the UCS and the UTS.

6.4 RESULTS AND DISCUSSION

6.4.1 Effect of fibre type

6.4.1.1 Static tests

The static tensile test results in Table 6.2 show the effect of yarn/fibre type on composite tensile strength. This has been previously discussed in *Chapter 3*. While J190 and H180 composites have similar UTS of 170-175 MPa, F20 composites exhibit significantly higher UTS of 236.3 \pm 12 MPa despite having lower fibre content. This is probably a result of three possibilities. Firstly, flax fibres have better

mechanical properties than jute and hemp fibres (Table 6.3). As jute and hemp have a better or similar cellulose content, cellulose crystallinity, degree of polymerisation (DP) and microfibril angle (MFA) in comparison to flax (Table 6.3), perhaps the significantly higher fibre aspect ratio of flax results in a higher fibre tensile strength [25-27]. McLaughlin et al. [28] and Mukherjee et al. [29] have statistically established the strong correlation between plant fibre structural parameters (cellulose content, MFA and aspect ratio) and their tensile properties (strength, modulus and elongation). Secondly, the F20 flax rovings used in this study have a significantly lower twist level than the J190 and H180 yarns. In *Chapter 5*, it has been shown that increasing reinforcement yarn twist has a quantifiable detrimental effect on composite tensile strength. For instance, composites made from J190 yarns (with yarn surface twist angle α of 20.5 ± 5.9) only receive 57% (= $\cos^2(2\alpha)$) of the fibre strength, while composites made from F20 rovings (with $\alpha = 0.5 \pm 0.1$) receive the entire fibre strength, due to no losses through reinforcement misorientation. Thirdly, plant fibre/yarn quality will affect the fibre and composite mechanical properties. Although both F20 and F50 composites have similar fibre content and are made from low-twist flax rovings/yarns, there is a 40% difference in their UTS. Madsen et al. [30, 31] and Baets et al. [32] have shown that an increasing number of defects and an increasing number of processing steps can reduce fibre/yarn quality and thus composite properties. It is encouraging to note that although mechanical properties of single plant fibres have high variability (Table 6.3), at a composite scale, the UTS of all the PFRPs have a small coefficient of variation between 4-6 %, which is similar to that of GFRPs (as confirmed in *Chapter 3*).

Table 6.3. Structural and mechanical properties of plant fibres [25-27].

| Fibre type | Cellulose content [%] | Cellulose crystallinity [%] | DP* | MFA [†] [°] | Aspect ratio | Tensile modulus [GPa] | Tensile strength [MPa] | Failure strain [%] |
|---------------|-----------------------------|-----------------------------------|------|-------------------------|-----------------|-----------------------------|------------------------------|--------------------------|
| Flax | 64–71 | 53-70 | 2420 | 5-10 | 1750 | 30-70 | 400-1100 | 2.7-3.2 |
| Hemp | 70–74 | 53-70 | 2300 | 2-6 | 900 | 30-60 | 300-800 | 1.3 - 2.7 |
| Jute | 61-72 | 53-70 | 1920 | 8 | 100 | 20-55 | 200-600 | 1.4-3.1 |

^{*}DP = degree of polymerization

[†]MFA = microfibril angle

6.4.1.2 Fatigue tests

Based on static tensile test results, the four different PFRPs were subjected to tension-tension (R = 0.1) fatigue tests at different stress levels (% of respective UTS). Fig. 6.4 presents S-N fatigue data for these PFRPs. The arrowhead at 1.4 x 10⁷ cycles indicates a 'run-out' test which did not fail. A gradual decline in fatigue strength with increasing number of fatigue cycles is observed. It is observed that the power-law model of Eq. 6.2 is a good fit to the experimental fatigue data; in fact all regressions have an R^2 -value > 0.95. This is generally characteristic of composites whose lifetime is dominated with matrix crack growth and inter-laminar cracking [22, 23]. Indeed, matrix cracks normal to the stress direction often occurred on the specimen surface early in the lifetime. The type of final failure observed in specimens tested in static tensile tests and tension-tension fatigue tests was similar; specimens failed in a catastrophic brittle manner with a jagged fracture surface and often showing delamination and longitudinal splits (sometimes reaching the tab area) that terminate and arrest at matrix surface crack(s). Unidirectional GFRPs and unidirectional carbon fibre composites are known to fail in a similar manner [22, 23, 33]. Fracture modes and surfaces are further discussed in Section 6.4.4.

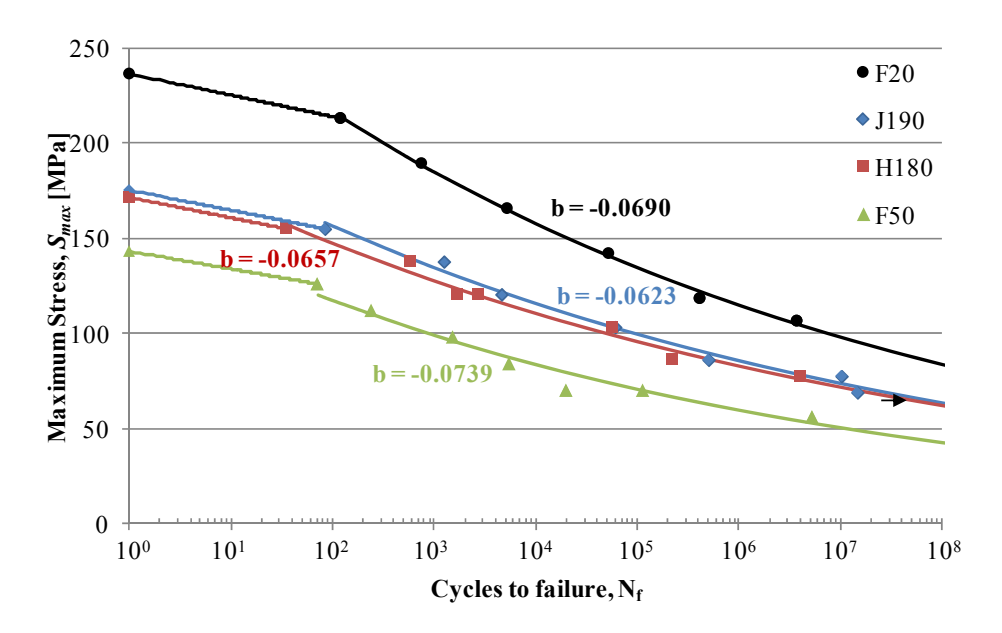


Fig. 6.4. Lifetime S-N diagram for polyester composites reinforced with different plant fibres/yarns. Power-law regression lines and the material fatigue strength coefficient (b-values) are also presented.

From the S-N diagram in Fig. 6.4 and Fig. 6.5, it is observed that although the static UTS of the PFRPs ranges from 140 to 240 MPa, the material fatigue strength coefficients b are very similar, ranging from -0.0739 to -0.0623. In fact, F20 composites have 40% higher static UTS than F50 composites, but similar rates of fatigue strength degradation (Fig. 6.5). This indicates that the fatigue failure mechanism in PFRPs, and the resulting gradual fatigue strength degradation, is independent of plant fibre/yarn type. This is possibly because jute, hemp and flax bast fibres are structurally very similar (Table 6.3) and the interfaces that form in thermoset composites reinforced with such fibres are also very similar. Hence, micro-crack growth rates at i) the fibre/matrix interface in the composite and ii) the cellulose/hemicellulose-lignin interface in the viscoelastic fibre (or fibre bundles) [5, 7] are similar. In his study on the fatigue behaviour of unidirectional flax and jute epoxy composites, Gassan [10] also noticed that the composites had very similar progressive damage propagation (indicated by SDC-load curves). These observations not only confirm that failure mechanisms in static and fatigue loading are dissimilar, but indeed that the static UTS can be used as an indicator of the lifetime fatigue performance of PFRPs. In essence, a PFRP with higher UTS usually has a higher load carrying capacity throughout its fatigue life, due to no detrimental effects to the strength degradation rate.

6.4.1.3 Comparison with GFRPs

Commonly, material S-N data is presented in normalised form on a plot of S_{max}/UTS against N (Fig. 6.5). Importantly, the material fatigue strength coefficient b remains the same. The normalised S-N diagram readily enables the comparison of the rate of fatigue strength degradation (b-values) of several materials. Fig. 6.5 not only presents normalised S-N data for the various unidirectional PFRPs, it also presents normalised S-N data for unidirectional GFRPs and carbon/epoxy. Data on the GFRPs material (v_f = 30% in [0]₅ lay-up, UTS = 570 MPa) is from extensive tests done by Prof. Mandell's group [17, 22, 23], while data on typical carbon/epoxy composites is from [34].

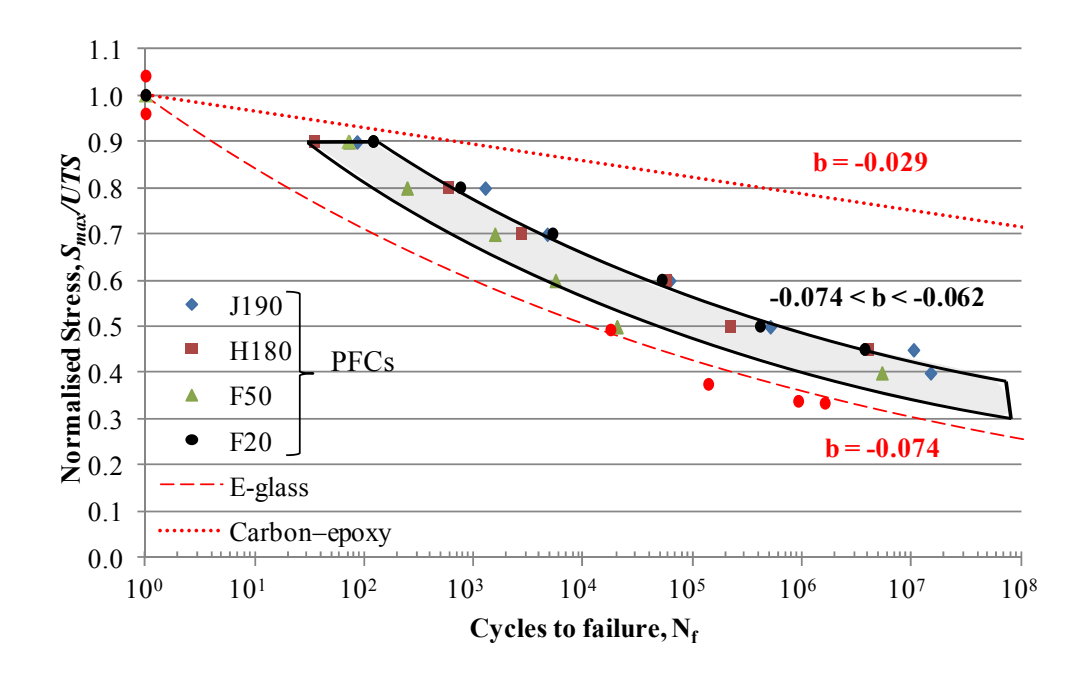


Fig. 6.5. Normalised S-N diagram comparing the tension-tension (R=0.1) fatigue performance of unidirectional thermoset matrix composites reinforced with plant (shaded), E-glass [22] and carbon [34] fibres.

From Fig. 6.5, it is immediately clear that unidirectional carbon/epoxy composites outperform both GFRPs and PFRPs in terms of fatigue properties. While carbon/epoxy composites have a value of $b \approx -0.029$, GFRPs and PFRPs have a much lower value of b. It is of great interest to observe that material fatigue strength coefficient of PFRPs ($b \approx -0.074$ to -0.062) is higher than or comparable to GFRPs ($b \approx -0.074$). This implies that damage development and fatigue strength degradation are relatively slower in PFRPs. Liang *et al.* [9] also find that in comparison to bidirectional flax composites, bidirectional GFRPs had a much steeper S-N curve, implying a more significant decrease in fatigue strength with respect to cycles to failure. Shahzad *et al.* [15] also confirm that randomly-oriented short-fibre hemp/polyester composites and chopped-strand GFRPs have a similar fatigue strength coefficient. However, it should be noted that aligned GFRPs have a much higher UTS than aligned PFRPs, and in terms of absolute stress, the fatigue and static properties of GFRPs is significantly better than that of PFRPs. This is clearly depicted in Fig. 6.6.

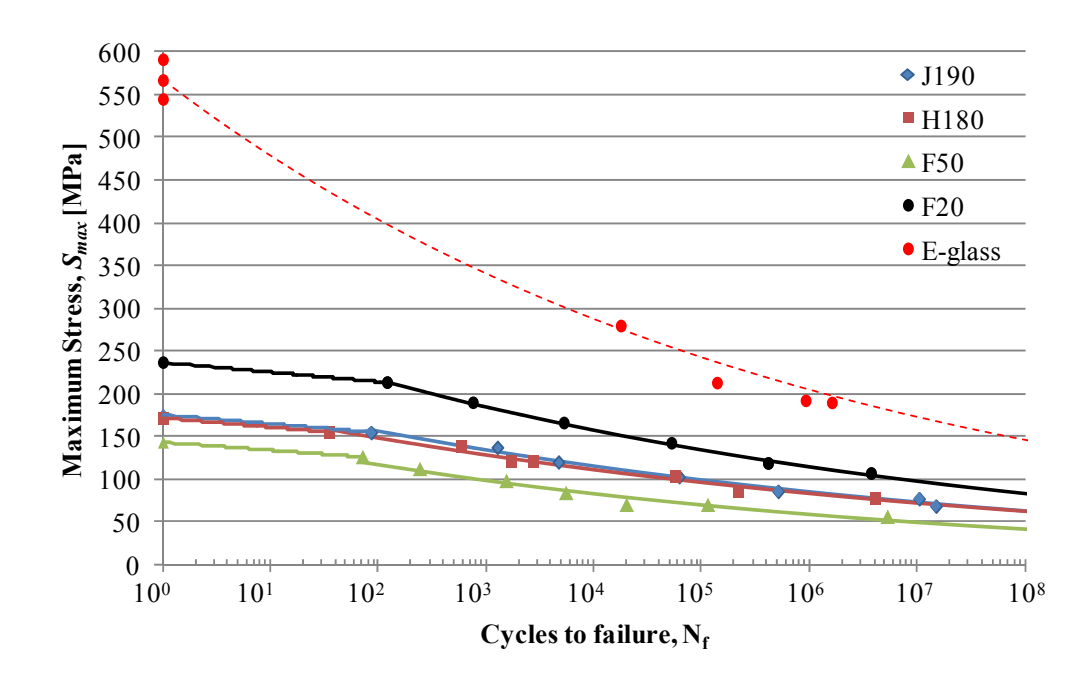


Fig. 6.6. S-N diagram comparing the tension-tension fatigue performance of UD PFRPs and UD GFRPs ($v_f = 30\%$ in $[0]_5$ lay-up, UTS = 570 MPa; material data from [22]).

While it is widely quoted that the fibre/matrix interface in PFRPs is weak due to poor adhesion between hydrophilic plant fibres and hydrophobic matrix [35-37], the interface in GFRPs has been optimised through sizing of glass fibres (specific to a resin system). Hence, it is surprising that damage accumulation rates in PFRPs are slower than in GFRPs. The causes of this behaviour are still unclear, however, there are three possible explanations. Firstly, several studies [4, 5, 9, 15] have shown that not only do plant fibres and their composites exhibit strain hardening when subjected to cyclic loads, but PFRPs also show much lower (if any at all) stiffness degradation over their fatigue life in comparison to GFRPs. As mentioned in Section 6.2, Liang et al. [9] observe that the loss of modulus of biaxial glass/epoxy composites is three times higher than that of flax/epoxy composites. It is known that the progressive reorientation of cellulose microfibrils in plant fibres towards the loading direction is the most plausible explanation for this observation [3, 4, 9]. In constant amplitude load-controlled fatigue tests, a gradual loss of modulus implies a gradual increase in strain amplitudes and thus faster damage accumulation. Perhaps, it is this ability of PFRPs to maintain stiffness over their fatigue life which imparts them with slow

damage accumulation rates. Secondly, the complex composite structure of viscoelastic plant fibres may provide them with crack absorbing and deflecting mechanisms [5, 7, 38]. This includes the ability of plant fibres to i) 'shed' layers of damaged structural cell walls [5, 7], ii) continually transfer loads onto adjacent layers and fibres [5, 7], iii) directly resist against delamination crack growth through interactions of the cellulose microfibrils and the hemicellulose-lignin matrix by imperfect microfibrillar alignment and subsequent microfibrillar bridging (relative to the crack plane) [7], and iv) reshape fibre cells into an ovular rather than circular cross-section [5], effectively increasing fibre aspect ratio and load-transferring ability [26]. Finally, plant fibres may be more capable of transferring stresses and strains to the matrix due to their rough surfaces. While glass fibres have a constant diameter across their length and have smooth surfaces, the diameter of plant fibres varies across their length and their surface is very rough. Sretenovic et al. [39] measured the development and distribution of strain in a single wood fibre-low density polyethylene composite by means of electronic laser speckle interferometry (ESPI). While it is typically expected that due to the different elastic modulus of the fibre and the matrix axial strain distribution is discontinuous across the fibre ends, they found that due to the roughness of wood fibre ends and the resulting larger effective surface area, the transition of strain from the fibre to the matrix was continuous. However, Sretenovic et al. [39] do acknowledge that pixel averaging effects in the ESPI method may cause the continuous strain distribution.

6.4.2 Effect of fibre volume fraction

Composite mechanical properties can often be tailored by changing, for instance, the fibre volume fraction. J190/polyester composites were manufactured at four different fibre volume fractions, ranging from 17 to 38%. The static tests results in Table 6.2 show that the UTS of J190/polyester increases linearly with fibre volume fraction (R² = 0.974), as per the rule of mixtures (*Chapter 4*). This shows that although different batches/types/quality of plant fibres may have variable properties, at a composite scale, PFRPs made from a single batch of fibre do follow conventional composite micro-mechanical models.

S-N data from tension-tension (R = 0.1) fatigue tests on these composites is presented in Fig. 6.7. Again, the power-law regressions are in good agreement with the experimental data ($R^2 > 0.95$). PFRPs with higher fibre content not only exhibit improved static (single cycle) properties, they also maintain higher fatigue load carrying capacities over their fatigue life. None of the S-N curves seem to be converging into each other before at least 10^{10} cycles, which is significantly higher than the number of stress cycles even wind turbine blades would face. In fact, the material fatigue strength coefficient b is fairly constant at $b \approx -0.0646$ for all the fibre volume fractions (Fig. 6.8), despite a small dip at $v_f = 25\%$. This implies that the slope of the S-N curves and the fatigue strength degradation rates are very similar. Hence, it can be concluded that increasing the fibre content of a PFRP is useful for improving both static and fatigue performance.

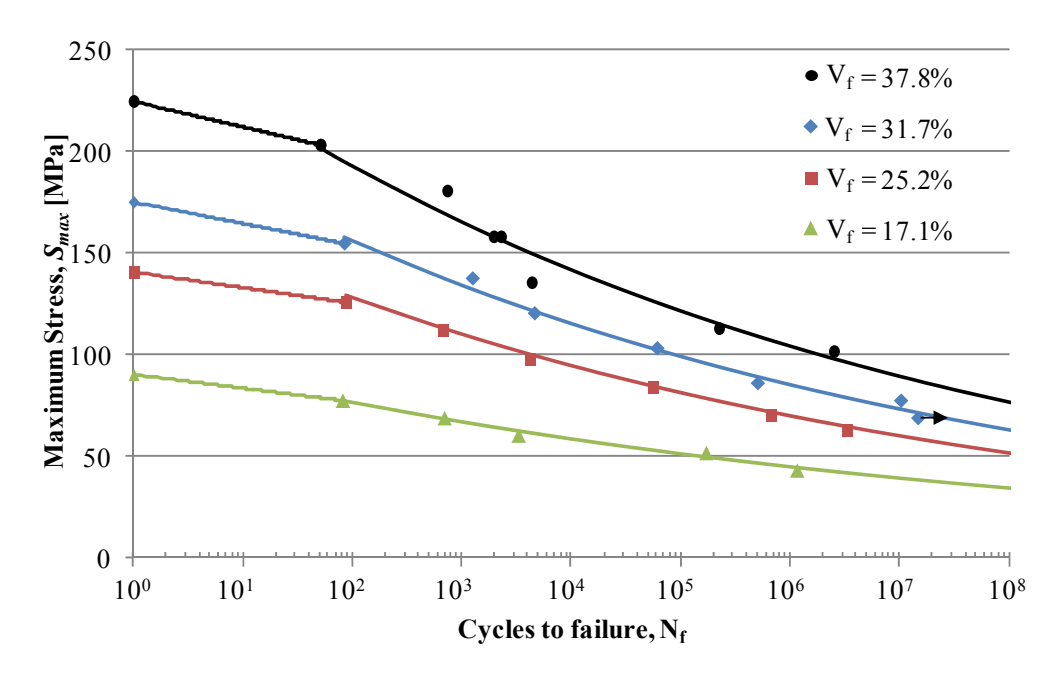


Fig. 6.7. S-N diagram showing fatigue life data for J190/polyester composites composing of different fibre volume fractions.

However, note that the fatigue behaviour up to only $v_f \approx 40\%$ has been investigated in this study. Several authors [1, 17, 40, 41] have shown that fatigue performance tends to degrade with increasing fibre content. This is because increased fibre content leads to *i*) more fibre/matrix interfaces, *ii*) more fibre-fibre interactions/contacts (as seen in

Chapter 6

Fig. 6.9) and iii) more regions of high local volume fractions due to increased yarn/strand compaction [42]. Although the interface enables stress transfer between the fibre and the matrix, it is also the region where the largest stress/strain gradients lie. Hence, the interface is the region where micro-cracks are most likely to grow and propagate. Increasing fibre content implies that fibres are now closer to each other and hence stress/strain gradients at the interface are even higher, leading to accelerated crack growth. In addition, touching fibres are likely sites for crack growth. Samborsky and Mandell [17, 41] have shown that increasing fibre content beyond 40-45% typically results in a drop in the fatigue strength coefficient b and thus poorer fatigue performance. Fig. 6.8 plots the variation in the fatigue strength coefficient b with increasing fibre content for triaxial GFRPs ([0, \pm 45,0] lay-up with 72%-0's; material data from [17]). Mandell et al. [42] have also demonstrated that while increasing the localised fibre volume fraction in a composite sample can improve static properties, it has a detrimental effect on the fatigue performance.

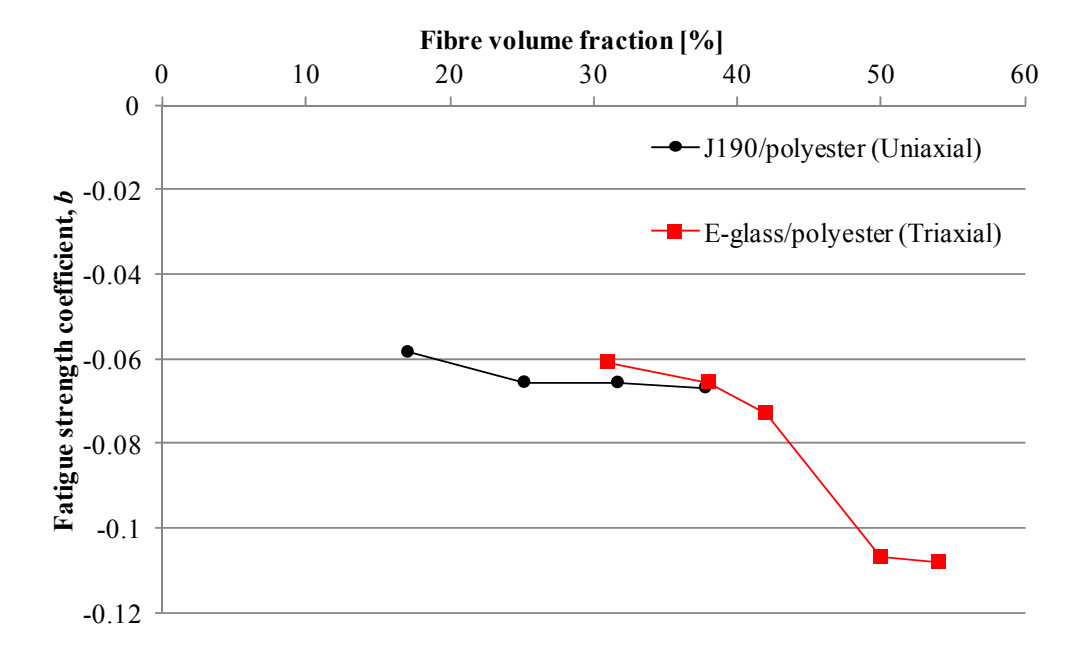


Fig. 6.8. Variation in the material fatigue strength coefficient b with fibre volume fraction, for J190/polyester and E-glass/polyester (material data from [17]).

As illustrated in Fig. 6.9, increasing the fibre content of J190/polyester composites affected the failure mechanism in tension-tension fatigue. At low fibre content, more matrix cracks formed at the specimen surface normal to the loading direction very early on in the fatigue life (Fig. 6.9a). Specimen failure was brittle, matrix dominated, with no longitudinal splitting and the fracture surface was flat with no delamination. At higher fibre volume fractions (Fig. 6.9b), fewer surface matrix cracks formed and specimen failure was brittle, catastrophic and with extensive fibre failure. The fracture surface was more jagged with extensive delamination and longitudinal splitting (even extending into the end tabs). Often, longitudinal splits extended into and arrested at a matrix surface crack normal to the loading direction. Interestingly, the fracture surfaces of specimen failed under static and fatigue loading were similar, which is typical in fatigue failure of composites [1, 17].

a) Matrix dominated failure at lower fibre content:
Matrix cracks normal to load, brittle fracture

1 mm
b) Fibre dominated failure at higher fibre content:
Splitting, delamination and jagged fracture surface

Fig. 6.9. Typical cross-section micrograph and failure modes of J190/polyester composites with a) low ($v_f = 17\%$) and b) high ($v_f = 38\%$) fibre content subjected to tension-tension fatigue loading. See text for details.

6.4.3 Effect of textile architecture

To characterise the influence of textile architecture on the fatigue performance of PFRPs, unidirectional ($[0]_4$ and $[90]_4$) and biaxial ($[\pm 45]_4$) F50/polyester composites were manufactured and tested. Static tensile results in Table 6.2 show that although the three composites have a similar fibre content, the UTS of $[0]_4$ composites is 11 and 3 times the UTS of $[90]_4$ and $[\pm 45]_4$ composites, respectively. Plant fibres are highly anisotropic due to their structure and composition. It follows that uniaxial composites reinforced with these plant fibres are also highly anisotropic. In fact, as has been revealed in *Chapter 5*, biaxial ($[\pm 45]_4$) PFRPs are a better option than uniaxial ($[0]_4$) PFRPs, for applications where loads are at an off-axis angle larger than 30°.

Fig. 6.10 illustrates the effect of textile architecture on the fatigue performance of F50/polyester composites. The power-law regressions are in good agreement with the experimental data ($R^2 > 0.95$). Increasing off-axis loading angle seems to improve the fatigue life at 90% of the UTS. While [± 45]₄ F50/polyester has a steeper S-N curve (lower value of b) in comparison to [0]₄ samples, [90]₄ has a flatter S-N curve. Fig. 6.10 clearly shows that under tension-tension load regime, textile architectures with fibre orientations off-axis to the loading direction result in a significant drop in composite static UTS which results in lower fatigue loading capacities throughout their fatigue life; that is, slight improvement in the fatigue strength coefficient does little to offset the reduction in UTS.

From Fig. 6.11, it is encouraging to see that fatigue strength degradation rate of $[\pm 45]_4$ F50/polyester is better than that of uniaxial ($[0]_5$ lay-up, $v_f = 30\%$, UTS = 570 MPa), biaxial ($[\pm 45]$ lay-up, $v_f = 28\%$, UTS = 139 MPa) and triaxial ($[0,\pm 45]$ lay-up with 48%-0's, $v_f = 36\%$, UTS = 361 MPa) GFRPs (material data from [17, 22]) for up to at least 10^8 cycles. This is due to i) the higher fatigue strength coefficient b and ii) the significantly better low-cycle fatigue properties, of PFRPs in comparison to GFRPs. Note that the ratio of the UTS of unidirectional and biaxial GFRPs is 4.1 (= 570/139), which is higher than that of unidirectional and biaxial F50/polyester (2.8 = 143/51).

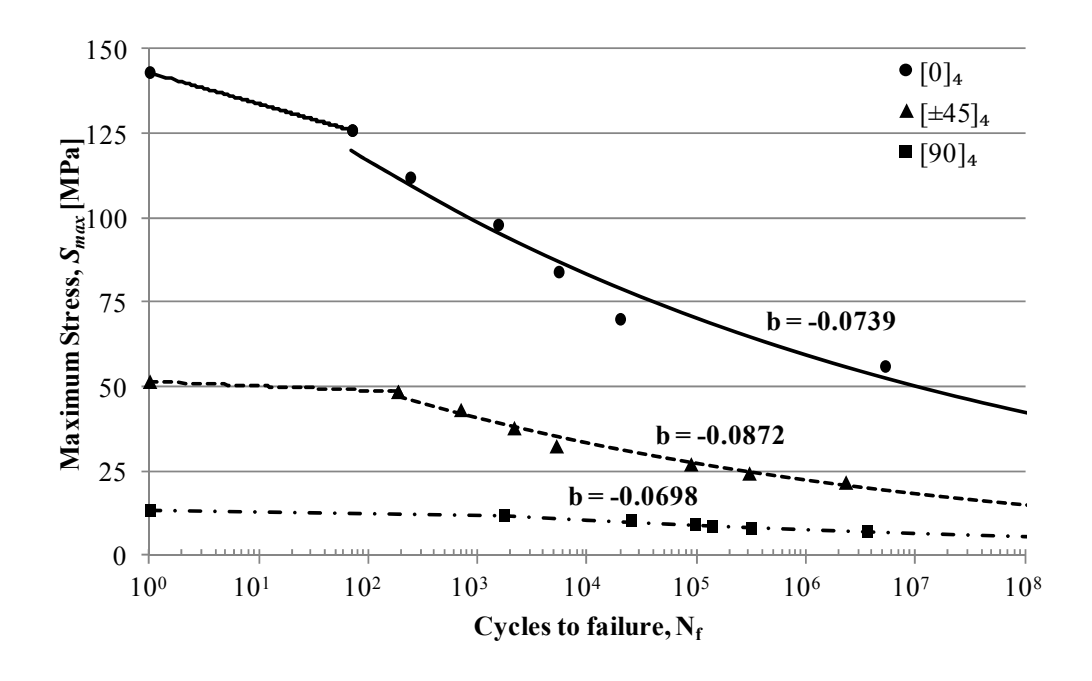


Fig. 6.10. S-N diagram showing fatigue life data for F50/polyester composites composing of different textile architectures.

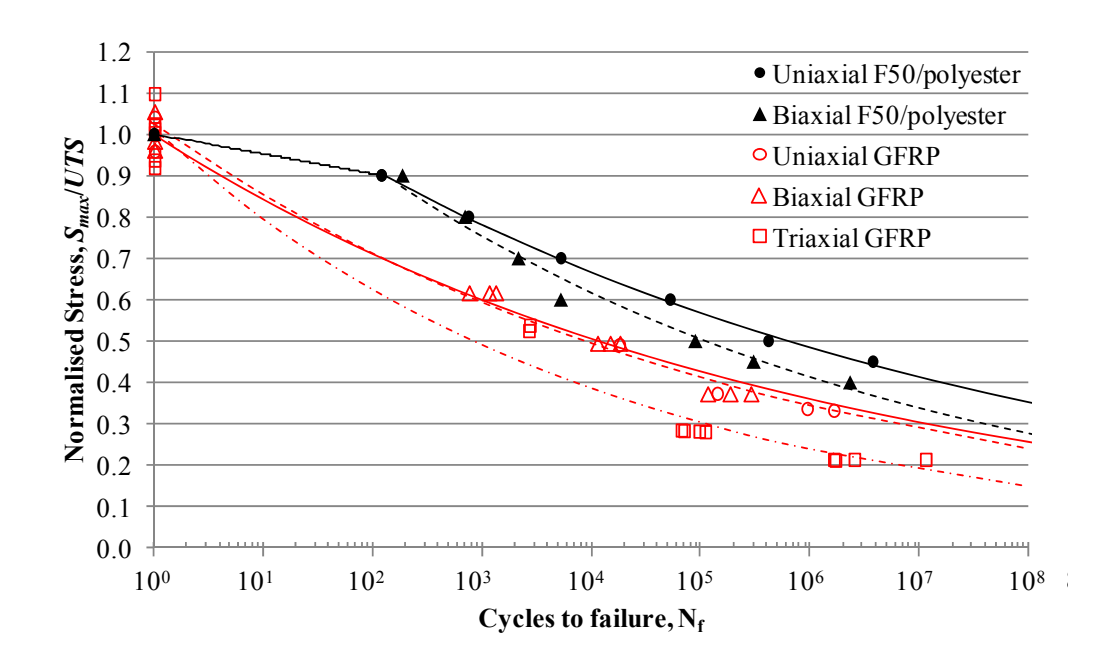


Fig. 6.11. Normalised S-N diagram comparing the tension-tension (R=0.1) fatigue performance of multi-axial composites reinforced with F50 and E-glass fibres.

In general, Fig. 6.11 shows that biaxial composites have a steeper S-N curve than unidirectional composites. Interestingly, traixial GFRPs has a higher fatigue strength degradation rate in comparison to both uniaxial and biaxial GFRPs. This is because the failure mechanism in triaxial composites is different to the failure mechanisms in uniaxial and biaxial composites. In triaxial composites, matrix cracking causes the $\pm 45^{\circ}$ layers to fail separately and then delaminate from the 0° material [22, 23]. This would also be expected from triaxial PFRPs.

Several researchers have studied the effect of off-axis loads and textile architecture on composite fatigue performance, including [10, 17, 22, 33, 43]. The most widely discussed topic is the difference in macroscopic failure morphology of (on-axis and off-axis) unidirectional and multi-axial composites, subjected to fatigue loads. Unidirectional composites subjected to on-axis (0°) loads fail due to fibre/matrix interfacial debonding and splitting along the fibre direction. Unidirectional composites subjected to off-axis loads (say 90°) fail at a single well-defined cross-section parallel to the fibre and thickness directions [33], typically due to cracks coalescing along interfaces [10]. On the other hand, biaxial composites typically fail due to matrix cracks forming and growing parallel to the fibres of each ply, followed by inter-laminar separation of the plies [17].

6.4.4 Effect of stress ratio

To generate a complete constant-life diagram for H180/polyester composites, they were systematically tested over five different stress ratios. From static tests, it is found that the UTS (170 MPa) is almost double the UCS (95 MPa). Fig. 6.12 plots the normalised stress-life data of the composites loaded at different stress ratios. While all power-law regression lines show strong fit to the experimental data ($R^2 > 0.97$), for tests in TC load range (R = -1) a piece-wise power-law regression is required as the composite hits a 'fatigue endurance limit' at about 10^4 cycles. Beyond this limit, cyclic stresses applied to the material (at R = -1) cause less fatigue damage. Although the fatigue strength drops drastically up to 10^4 cycles, it is encouraging to observe an endurance limit so early on in the fatigue life of H180 composites

subjected to fully-reversed (R= -1) cyclic loads as this is the most severe fatigue load regime.

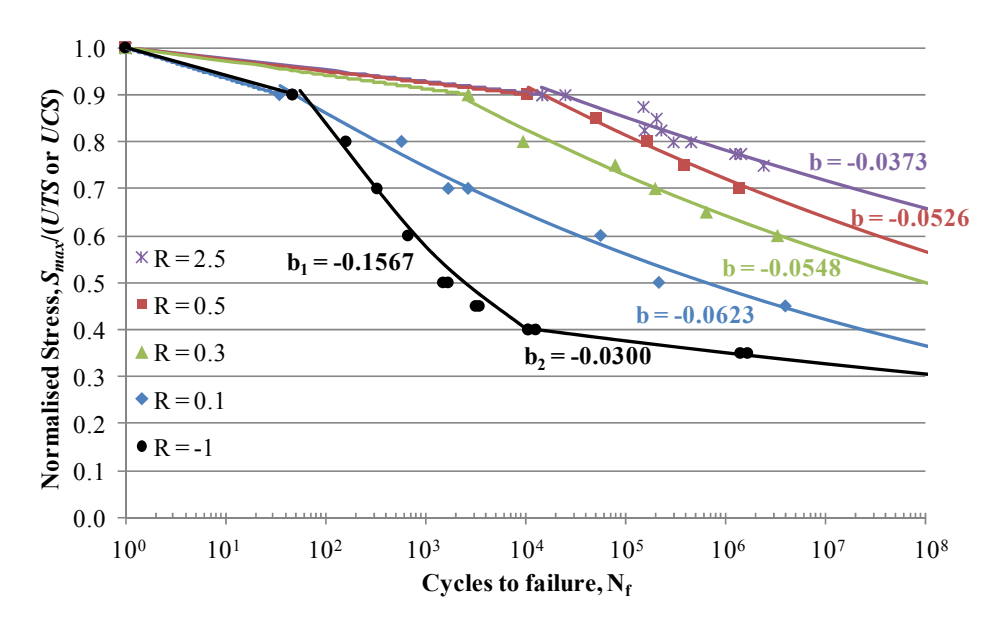


Fig. 6.12. Normalised S-N diagram showing the effect of stress ratio on fatigue life of H180/polyester composites. Data for TT mode is normalised by the UTS, while data for TC and CC mode is normalised by the UCS.

Fig. 6.12 shows that increasing the stress ratio R substantially increases the fatigue life at high stresses. For instance, when constant amplitude cyclic loads are applied at stress ratios R of -1, 0.1, 0.3, 0.5 and 2.5 at $S_{max}/(\text{UTS}$ or UCS) of 70%, according to the regression equations based on the experimental data, H180 composites would survive 2.8×10^2 , 2.7×10^3 , 2.1×10^5 , 1.8×10^6 , and 1.9×10^7 cycles. That is, the fatigue life increases by at least a decade of cycles for every stress ratio. In addition, increasing the stress ratio R increases the material fatigue strength coefficient b. A similar trend is also observed for GFRPs materials [17, 41, 44]. This implies that increasing the stress ratio R leads to a flatter S-N curve on a logS-logN plot and essentially, slower fatigue degradation and damage accumulation rates. A possible explanation for this is that increasing the stress ratio R, reduces the stress amplitude S_{amp} (for a constant maximum (absolute) stress S_{max})) of the load regime. The load spectrum in Fig. 6.2 shows this graphically. At higher stress ratios, the material is being subjected to lower stress amplitudes, and hence it will have to endure lower

Chapter 6

stress/strain gradients in the fibre, matrix and at the fibre/matrix interface. This would in turn lead to reduced crack growth rates and less significant fatigue strength degradation with increasing number of cycles.

The stress ratio also has an effect on the failure mode of the composites. Example failure surfaces from tests in the different load ranges are shown in Fig. 6.13. Composites tested under TT mode (R = 0.1, 0.3 and 0.5) fail in a brittle manner including extensive fibre fracture, matrix cracking, delamination and longitudinal splitting (Fig. 6.13a). Crack growth, in this case, is a result of Mode 1 (opening mode) and Mode 2 (in-plane shear mode) crack loading [22]. Importantly, single plant fibres subjected to TT fatigue loads also experience mode mixities (Mode 1 and Mode 2), although Mode 1 prevails due to lower fracture resistance [7]. Composites tested under TC (R = -1) and CC (R = 2.5) load range display the typical single-kink failure and wedge-shaped failure, respectively. Mode 2 (in-plane shear mode) should be the dominant crack loading mechanism for TC and CC load ranges [22]. In TC load range, the specimen fails when a kink develops at a plane 45° to the loading direction (Fig. 6.13b) due to pure in-plane shear resulting from each half sliding over the other half. Specimen failure in CC load range occurs in the form of a symmetrical double-kink (Fig. 6.13c) resulting from both halves forcing into each other and folding on the same side.

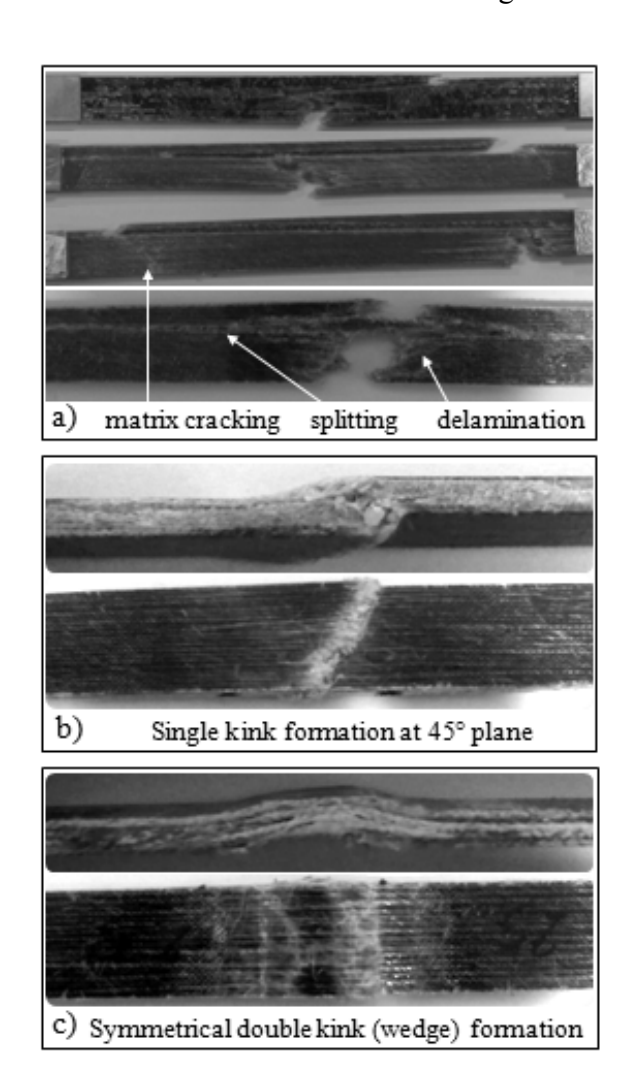


Fig. 6.13. Typical failure modes of PFRPs loaded in *a)* tension-tension load range, *b)* tension-compression load range and *c)* compression-compression load range. See text for details.

6.4.5 Constant-life diagram

The power-law regression equations describing the trend in the fatigue lifetime data over different stress ratios can be used to plot a constant-life diagram. This is typically a graph of stress amplitude S_{amp} against mean stress S_{mean} . Each curve on the graph is a 'line of constant life'. Fig. 6.14 shows a complete Haigh constant-life diagram that has been constructed for H180/polyester composites. The power-law regression curves have been extrapolated to 10^9 cycles to failure. Obviously, the accuracy of this diagram can be improved by testing more samples at more stress ratios. Although the UCS of H180/polyester is half the UTS, the CC fatigue

Chapter 6

behaviour is impressive due to the high fatigue strength coefficient b (flatter logSlogN curve). In fact, except the low-cycle (N < 10^3) fully-reversed (R = -1) TC fatigue performance, PFRPs offer very stable and useful fatigue properties.

The constant-life diagram in Fig. 6.14 can be used for the life prediction of a component made from H180/polyester, given that the loads the component is subjected to are known. For instance, if a component made from unidirectional H180/polyester has to sustain (S_{mean} , S_{amp}) of (90, 20), the component will survive $\sim 10^8$ cycles. Recently, the author of this thesis has applied this constant-life diagram for the fatigue design and life prediction of a 3.5-meter hemp/polyester small wind turbine blade [18, 19].

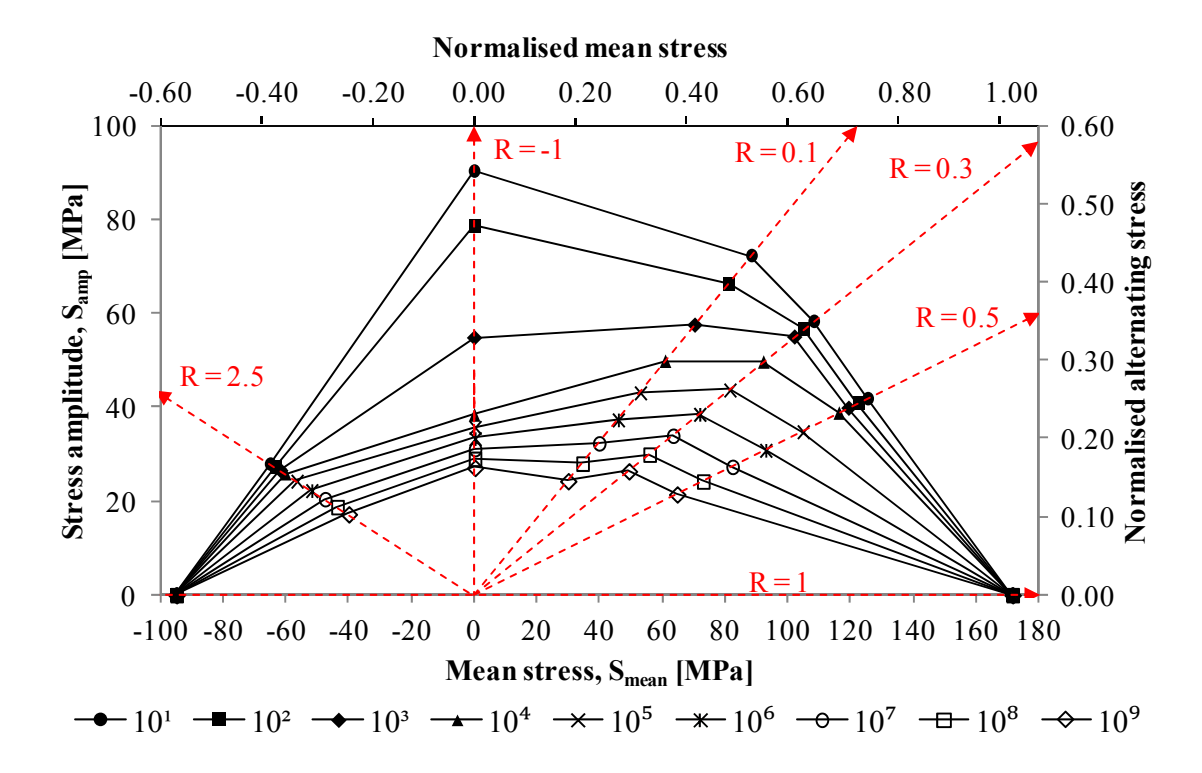


Fig. 6.14. Constant-life diagram for H180/polyester composites. The secondary axes have been normalised to the UTS (171.3 MPa).

Often constant-life diagrams are presented in normalised form (Fig. 6.14), where both axes are normalised to the bigger of the static tensile or compressive strength. This allows the use of the constant-life diagram for life prediction of components made from another material whose fatigue behaviour (depicted by S-N curves) is Page | 196

similar [44, 45]. In Section 6.4.1.2 it was concluded that the fatigue performance of PFRPs is independent of fibre type, due to the several chemical, structural and mechanical similarities in bast fibres. Hence, using the normalised axes scales, Fig. 6.14 could be used for the fatigue life prediction of a component made from flax/polyester, for example.

Mandell *et al.* [41, 44] have produced constant-life diagrams for an E-glass/epoxy laminate ([$\pm 45/0_2$] lay-up with 64%-0°, $v_f = 53\%$), up to 10^7 cycles to failure. The UTS and UCS of this laminate are 843 MPa and -687 MPa, respectively. Due to the significantly higher static properties of GFRPs compared to PFRPs, the fatigue properties of GFRPs is far superior to PFRPs. In fact, the constant-life diagram of GFRPs is almost 4-fold that of H180/polyester.

6.5 Conclusions

There is a noticeable lack of fatigue data on plant fibre composites (PFRPs) which seriously limits their prospective use in fatigue critical components. The objective of this chapter was to provide a complete set of fatigue data on vacuum-infused aligned PFRPs. S-N lifetime diagrams have been constructed to specifically investigate the effect of *i*) plant fibre type/quality, *ii*) fibre volume fraction, *iii*) textile architecture, and *iv*) stress ratio, on PFRP cyclic loading behaviour. At each stage, the fatigue performance of PFRPs has been compared to that of GFRPs (material data from [17]). To facilitate fatigue design and life prediction of a PFRP component, a complete constant-life diagram has been generated.

It has been demonstrated that power-law regression lines are a good fit to S-N fatigue data for PFRPs ($R^2 > 0.95$), and thus useful in predicting the fatigue life of PFRPs. While plant fibre type, plant fibre quality, textile architecture and composite fibre content have a significant impact on the static (tensile) properties of the PFRP, they have little impact on the material fatigue strength coefficient b (which dictates the slope of the S-N curve). In essence, higher static properties are a sign of superior fatigue loading capacities throughout the lifetime of PFRPs. Increasing stress ratios lead to improved fatigue performance (increasing b) in PFRPs. Fatigue fracture mechanisms and modes are the same for all plant fibre types, but depend on fibre

content, textile architecture and load regimes (stress ratios). Although the absolute fatigue performance of GFRPs is far superior to PFRPs, it is a revelation to find that fatigue strength degradation rates are lower in PFRPs than in GFRPs.

6.6 REFERENCES

- 1. Nijssen R. Fatigue life prediction and strength degradation of wind turbine rotor blade composites. PhD, 2006. Delft University: Delft, Netherlands.
- 2. Shahzad A. *Impact and fatigue properties of natural fibre composites*. PhD, 2009. Swansea University: Swansea, UK.
- 3. Spatz H, Kohler L, Niklas KJ. Mechanical behaviour of plant tissues: composite materials or structures? *The Journal of Experimental Biology*, 1999, 202: p. 3269–3272.
- 4. Baley C. Analysis of the flax fibres tensile behaviour and analysis of the tensile stiffness increase. *Composites Part A: Applied Science and Manufacturing*, 2002, 33: p. 939-948.
- 5. Silva F, Chawla N, Filho RDDT. An experimental investigation of the fatigue behaviour of sisal fibers. *Materials Science and Engineering A*, 2009, 516: p. 90-95.
- 6. Mandell J, McGarry FJ, Hsieh AJY, Li CG. Tensile fatigue of glass fibers and composites with conventional and surface compressed fibers. *Polymer Composites*, 1985, 6(3): p. 168-174.
- 7. Hamad W. On the mechanisms of cumulative damage and fracture in native cellulose fibres. *Journal of Materials Science Letters*, 1998, 17: p. 433-436.
- 8. Harris B. *Engineering composite materials*, 1999. London: The Institute of Materials.
- 9. Liang S, Gning, PB, Guillaumat, L. A comparative study of fatigue behaviour of flax/epoxy and glass/epoxy composites. *Composites Science and Technology*, 2012, 72(5): p. 535-543.
- 10. Gassan J. A study of fibre and interface parameters affecting the fatigue behaviour of natural fibre composites. *Composites Part A: Applied Science and Manufacturing*, 2002, 33: p. 369-374.
- 11. Gassan J, Bledzki AK. Possibilities for improving the mechanical properties of jute/epoxy composites by alkali treatment of fibres. *Composites Science and Technology*, 1999, 59: p. 1303-1309.
- 12. Towo A, Ansell MP. Fatigue of sisal fibre reinforced composites: Constant-life diagrams and hysteresis loop capture. *Composites Science and Technology*, 2008, 68: p. 915-924.
- 13. Towo A, Ansell MP. Fatigue evaluation and dynamic mecahnical thermal analysis of sisal fibre-thermosetting resin composites. *Composites Science and Technology*, 2008, 68: p. 925-932.
- 14. Yuanjian T, Isaac, DH. Impact and fatigue behaviour of hemp fibre composites. *Composites Science and Technology*, 2007, 67: p. 3300-3307.
- 15. Shahzad A, Isaac DH. Fatigue properties of hemp fibre composites, in 17th International Conference on Composite Materials (ICCM-17). 2009. Edinburgh, UK.
- 16. Shahzad A. Effects of alkalization on tensile, impact, and fatigue properties of hemp fiber composites. *Polymer Composites*, 2012, 33(7): p. 1129-1140.
- 17. Samborsky D. Fatigue of E-glass fiber reinforced composite materials and substructures. MSc, 1999. Montana State University: Bozeman.

- 18. Shah D, Schubel PJ, Clifford MJ, Licence P. Fatigue characterisation of plant fibre composites for small-scale wind turbine blade applications, in *5th Innovative Composites Summit JEC Asia 2012*. 26-28 June 2012. Singapore.
- 19. Shah D, Schubel PJ, Clifford MJ, Licence P. Fatigue characterisation of plant fibre composites for rotor blade applications, in JEC Composites Magazine, No. 73: Special JEC Asia, June 2012. JEC Composites: Paris. p. 51-54.
- 20. *BS ISO 13003:2003*, *Fibre-reinforced plastics Determination of fatigue properties under cyclic loading conditions*, 2003. British Standards Institution: London.
- 21. Gassan J, Bledzki AK. The influence of fiber-surface treatment on the mechanical properties of jute-polypropylene composites. *Composites Part A: Applied Science and Manufacturing*, 1997, 28A: p. 1001-1005.
- 22. Mandell J, Reed RM, Samborsky, DD. *SAND92-7005*, Fatigue of fiberglass wind turbine blade materials, 1992. Sandia National Laboratories.
- 23. Mandell J, Reed RM, Samborsky DD, Pan Q. Fatigue performance of wind turbine blade composite materials. *Wind Energy*, 1993, 14: p. 191-198.
- 24. Bach P. *ECN-C-92-072*, Fatigue properties of glass and glass/carbon-polyester composites for wind turbines, 1992. Netherlands Energy Research Foundation ECN: Petten.
- 25. Lewin M. *Handbook of fiber chemistry*. Third ed, 2007. Boca Raton: CRC Press LLC.
- 26. Pickering K, ed. *Properties and performance of natural-fibre composites.* 2008. CRC Press LLC: Boca Raton.
- 27. Madsen B. *Properties of plant fibre yarn polymer composites An experimental study*. PhD, 2004. Technical University of Denmark: Lyngby, Denmark.
- 28. McLaughlin E, Tait RA. Fracture mechanism of plant fibres. *Journal of Materials Science*, 1980, 15: p. 89-95.
- 29. Mukherjee P, Satyanarayana KG. An empirical evaluation of structure-property relationships in natural fibres and their fracture behaviour. *Journal of Materials Science*, 1986, 21: p. 4162-4168.
- 30. Madsen B, Mehmood S, Aslan M. Variability in properties of natural fibres, in *NATEX Workshop*. 2012. Chesterfield, UK.
- 31. Hanninen T, Thygesen A, Mehmood S, Madsen B, Hughes M. Mechanical processing of bast fibres: The occurrence of damage and its effect on fibre structure. *Industrial Crops and Products*, 2012, 39: p. 7-11.
- 32. Baets J, Plastria D, Ivens J, Verpoest I. Determination of the optimal flax fibre preparation for use in UD-epoxy composites, in *4th International Conference on Sustainable Materials, Polymers and Composites.* 6-7 July 2011. Birmingham, UK.
- 33. Kawai M, Yajima S, Hachinohe A, Takano Y. Off-axis fatigue behaviour of unidirectional carbon fiber-reinforced composites at room and high temperatures. *Journal of Composite Materials*, 2001, 35: p. 545-575.
- 34. Manwell J, McGowan J, Rogers A. *Wind energy explained: Theory, design and application, Second edition*, 2009. Chichester: John Wiley and Sons, Ltd.
- 35. Kalia S, Kaith BS, Kaur I. Pretreatments of natural fibers and their application as reinforcing material in polymer composites a review. *Polymer Engineering and Science*, 2009, 49(7): p. 1253-1272.
- 36. Mwaikambo L, Ansell MP. Chemical modification of hemp, sisal, jute and kapok fibers by alkalization. *Journal of Applied Polymer Science*, 2002, 84: p. 2222-2234.
- 37. John M, Anandjiwala RD. Recent developments in chemical modification and characterization of natural fiber-reinforced composites. *Polymer Composites*, 2008: p. 187-207.

- 38. Nosti J. Performance analysis and life prediction for small wind turbine blades: A wood laminate case study, 2009. California Polytechnic State University: San Luis Obispo.
- 39. Sretenovic A, Muller U, Gindl W. Mechanism of stress transfer in a single wood fibre-LDPE composite by means of electronic laser speckle interferometry. *Composites Part A: Applied Science and Manufacturing*, 2006, 37: p. 1406-1412.
- 40. Boller K. *ML-TDR-64-86*, Effect of tensile mean stresses on fatigue properties of plastic laminates reinforced with unwoven glass fibers, 1964. Air Force Materials Laboratory: Dayton.
- 41. Mandell J, Samborsky DD, Agastra P. Composite materials fatigue issues in wind turbine blade construction, in *SAMPE 2008*. 2008. Long Beach.
- 42. Mandell J, Samborsky DD, Sutherland HJ. Effects of materials parameters and design details on the fatigue of composite materials for wind turbine blades, in *European Wind Energy Conference*. 1999. Nice, France.
- 43. van Den Oever M, Peijs T. Continuous-glass-fibre-reinforced polypropylene composites- II. Influence of maleic-anhydride modified polypropylene on fatigue behaviour. *Composites Part A: Applied Science and Manufacturing*, 1998, 29A: p. 227-239.
- 44. Samborsky D, Wilson TJ, Mandell JF. Comparison of tensile fatigue resistance and constant life diagrams for several potential wind turbine blade laminates, 2006. American Institute of Aeronautics and Astronautics: Reston.
- 45. Mandell J, Samborsky DD, Wahl NK, Sutherland HJ. Testing and analysis of low cost composite materials under spectrum loading and high cycle fatigue conditions, in 14th International Conference on Composite Materials (ICCM-14). 2003. San Diego.